ChemPubSoc Europe

DOI: 10.1002/chem.201405679

CHEMISTRY
A European Journal
Full Paper

Cluster Compounds

What Controls the Magnetic Exchange Interaction in Mixed- and Homo-Valent Mn_7 Disc-Like Clusters? A Theoretical Perspective

Kuduva R. Vignesh,[b] Stuart K. Langley,[c] Keith S. Murray,[c] and Gopalan Rajaraman*[a]

Abstract: Density functional theory (DFT) studies have been undertaken to compute the magnetic exchange and to probe the origin of the magnetic interactions in two hetero- and two homo-valent heptanuclear manganese disc-like clusters, of formula $[Mn^{II}_4Mn^{IV}_3(tea)(teaH_2)_3(peolH)_4]$ (**1**), $[Mn^{II}_4Mn^{III}_3F_3(tea)(teaH)(teaH_2)_2(piv)_4(Hpiv)(chp)_3]$ (**2**), $[Mn^{II}_7(pppd)_6(tea)(OH)_3]$ (**3**) and $[Mn^{II}_7$ $(paa)_6(OMe)_6]$ (**4**) ($teaH_3$ = triethanolamine, $peolH_4$ = pentaerythritol, Hpiv = pivalic acid, Hchp = 6-chloro-2-hydroxypyridine, pppd = 1-phenyl-3-(2-pyridyl) propane-1,3-dione; paaH = *N*-(2-pyridinyl)acetoacetamide). DFT calculations yield *J* values, which reproduce the magnetic susceptibility data very well for all four complexes; these studies are also highlighting the likely ageing/stability problems in two of the complexes. It is found that the spin ground states, *S*, for complexes **1**–**4** are drastically different, varying from $S = 29/2$ to $S = 1/2$. These values are found to be controlled by the nature of the oxidation state of the metal ions and minor differences present in the structures. Extensive magneto–structural correlations are developed for the seven building unit dimers present in the complexes, with the correlations unlocking the reasons behind the differences in the magnetic properties observed. Independent of the oxidation state of the metal ions, the Mn-O-Mn/Mn-F-Mn angles are found to be the key parameters, which significantly influence the sign as well as the magnitude of the *J* values. The magneto–structural correlations developed here, have broad applicability and can be utilised to understand the magnetic properties of other Mn clusters.

Introduction

Transition-metal clusters have received a great deal of attention over the last decade as certain molecules exhibit magnetic bistability, an important feature that is purely molecular in origin. Several exciting potential applications have since been envisaged, such as high density information storage devices, quantum computing, magnetic refrigeration and spintronic devices.[1] These molecules, which exhibit slow relaxation of magnetisation in the absence of a magnetic field, are commonly called single molecule magnets (SMMs) and act as magnets below their blocking temperature (T_B).[2] Requirements for a molecule to exhibit SMM behaviour include a high-spin ground state (*S*), with a negative zero-field splitting (ZFS) parameter *D*. Other desirable properties include negligible intermolecular magnetic interactions, large pair-wise magnetic exchange and a low probability for quantum tunnelling of the magnetisation (QTM). The combination of *S* and *D* results in an energy (anisotropy) barrier (*U*) to the reversal of the magnetisation vector, which depends directly on the square of the spin, and on its magnetic anisotropy (DS_z^2). This leads to a case where upon application and removal of a magnetic field the system can be stabilised in one of the high-spin energy wells.[2b] Since the report of the Mn_{12}Ac cluster,[3] hundreds of SMMs containing transition-metal ions have been reported. Of notable interest is a $[Mn^{III}_6]$ SMM reported with a barrier height of 86 K; the largest for any polynuclear manganese complex reported to date.[4] Besides transition metals, lanthanide-based complexes have contributed significantly to the area of SMMs, with blocking temperatures as high as 14 K being achieved.[5] For the design of transition-metal-based SMMs, polynuclear manganese complexes are favoured as they offer large Ising-type anisotropy, with complexes often yielding a large spin ground state; with values as high as $S = 83/2$ reported.[6] Although hundreds of Mn-based SMMs have now been reported, the field of SMM materials is still in its nascent stages and the magnetic properties are not often predictable. Another challenging aspect, especially for very large coordination complexes is that fitting/modelling of the experimental magnetic data is difficult. Understanding the nature of the individual pair wise super-exchange interactions within larger motifs are of vital importance. These interactions determine the overall

[a] *Prof. G. Rajaraman*
Department of Chemistry
Indian Institute of Technology Bombay
Powai, Mumbai, Maharashtra, 400 076 (India)
Fax: (+91) 22-2576-7152
E-mail: rajaraman@chem.iitb.ac.in

[b] *K. R. Vignesh*
IITB-Monash Research Academy
IIT Bombay, Mumbai, 400076 (India)

[c] *Dr. S. K. Langley, Prof. K. S. Murray*
School of Chemistry
Monash University
Victoria, 3168 (Australia)

Supporting information for this article is available on the WWW under http://dx.doi.org/10.1002/chem.201405679.

magnetic susceptibility behaviour and, if understood, can potentially allow us to design SMMs with a greater control of the ground spin value. Manganese clusters, in particular, with the accessibility of various oxidation states, such as +2, +3 and +4 often lead to a complex exchange topology, enhancing the need to incorporate a greater number of parameters to fit the data. In many cases, however, fits are precluded. Theoretical tools, particularly those based on density functional methods, have emerged as a powerful tool for the computation of magnetic exchange coupling in large polynuclear complexes[6b,7] and of other spin Hamiltonian parameters.[8] In earlier work we have utilised these methods to predict the pair wise magnetic interaction in dinuclear $[Mn^{III}_2(OR)_2]$ complexes, relating the magnetic interactions to the orientation of Jahn–Teller axes. Studies on dinuclear mixed-valence manganese species are, however, scarce.[7d,9]

A favourable metal topology which has been observed in manganese cluster chemistry is a planar or near planar, heptanuclear disc-like metallic core.[10] These complexes are made up of a central metal ion surrounded by a ring of six ions. This disc topology is sought after mainly because such a complex often displays a very large spin ground state.[10a,b] The most commonly reported manganese disc complexes are heterovalent Mn^{II} and Mn^{III} compounds,[10] but homo-valent Mn^{II} clusters have also been reported.[11] In the mixed-valence cases, spin values ranging from $S=17/2$ to $S=16$ are found. This topology is not only restricted to manganese however, and is also reported for other transition metals, such as homo-valent Co^{II} and mixed-valent $Co^{II/III}$ systems, all of which display SMM behaviour.[8c,12] Other disc-like complexes containing $[Fe^{II/III}$ or $Fe^{III}]$[13] and $[Ni^{II}$ or $Ni^{II/III}]$[14] ions have also been synthesised, as well as larger discs such as $[Mn_{10}]$, $[Mn_{14}]$,[15] $[Fe^{III}_{17}]$, $[Fe^{III}_{19}]$[16] and $[Co_{24}]$[17] complexes, all of which exhibit large spin ground states.

Despite extensive experimental work, theoretical efforts towards understanding the magnetic coupling in large mixed-valence manganese clusters are rare.[10a,b,18] As the oxidation state is likely to play a decisive role in controlling the magnetic properties, here we have undertaken detailed theoretical studies on four $[Mn_7]$ disc complexes possessing variable oxidation states and structural features. DFT calculations are performed on two mixed-valent complexes; $[Mn^{II}_4Mn^{IV}_3(tea)(teaH_2)_3(peolH)_4]$ (**1**), see Figure 1 a, ($teaH_3$ = triethanolamine, $peolH_4$ = pentaerythritol) and $[Mn^{II}_4Mn^{III}_3F_3(tea)(teaH)(teaH_2)_2(piv)_4(Hpiv)(chp)_3]$ (**2**), see Figure 1 b, (Hpiv = pivalic acid, Hchp = 6-chloro-2-hydroxypyridine) reported by some of us earlier.[19] Compound **1** was the first example of a heptanuclear disc with a $[Mn^{II}_4Mn^{IV}_3]$ oxidation-state distribution, compound **2** displays a unique arrangement of oxidation states within the disc when compared to other known $\{Mn^{II}_4Mn^{III}_3\}$ examples. We then extend our calculations to two homo-valent complexes, these are, $[Mn^{II}_7(pppd)_6(tea)(OH)_3]$ (**3**), see Figure 2 a, (pppd = 1-phenyl-3-(2-pyridyl)propane-1,3-dione) and $[Mn^{II}_7(paa)_6(OMe)_6]$ (**4**), see Figure 2 b, (paaH = N-(2-pyridinyl) acetoacetamide)[20] in order to probe the role the Mn oxidation state plays in controlling the magnetic properties of these clusters. It was found experimenatlly that the spin ground state S varies from 29/2 to 5/2 for compounds **1**–**4** and therefore a theoretical approach was undertaken in an attempt to explain these differences and provide an underlying reason for the magnetic interactions observed.

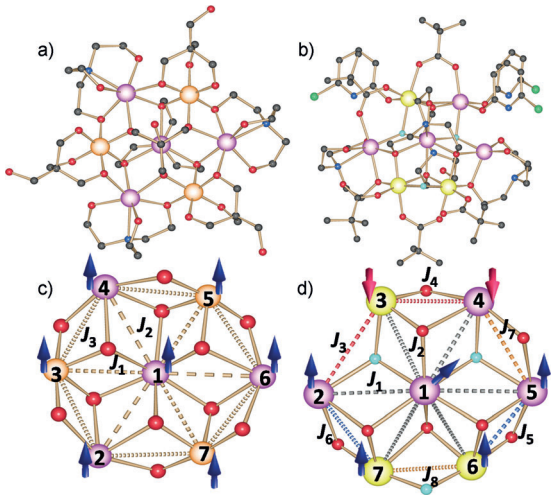

Figure 1. a) Molecular structure of compound **1** (colour scheme: Mn^{II} = pink, Mn^{IV} = orange, O = red, N = blue, C = black). b) Molecular structure of compound **2** (colour scheme: Mn^{II} = pink, Mn^{III} = yellow, F = cyan, Cl = green). c) Magnetic exchange pathways in compound **1** determined by using DFT calculations. d) Magnetic exchange pathways in compound **2** determined by using DFT calculations. Up and down arrows indicate spin-up and spin-down configurations predicted, respectively, with the tilted arrow in d) indicating the competing interactions present.

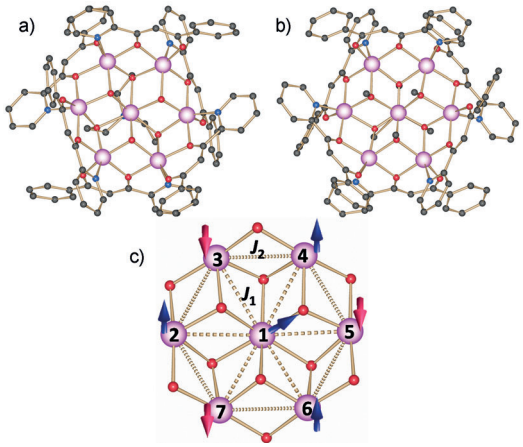

Figure 2. Molecular structures of a) compound **3** and b) compound **4** (colour scheme: Mn^{II} = pink, O = red, N = blue, C = black) (the hydrogen atoms are omitted for clarity). c) Magnetic exchange pathways in complexes **3** and **4** determined by using DFT calculations.

Computational Details

The manganese ions in compounds **1** (Mn^{II} = pink and Mn^{IV} = orange) and **2** (Mn^{II} = pink and Mn^{III} = yellow) are labelled as shown in Figure 1. The following exchange Hamiltonian has been employed to evaluate the magnetic exchange interactions in compound **1** [Eq. (1)].

$$\hat{H} = -\begin{bmatrix} 2J_1(S_{Mn1}S_{Mn3} + S_{Mn1}S_{Mn5} + S_{Mn1}S_{Mn7}) \\ +2J_2(S_{Mn1}S_{Mn2} + S_{Mn1}S_{Mn4} + S_{Mn1}S_{Mn6}) \\ +2J_3\begin{pmatrix} S_{Mn2}S_{Mn3} + S_{Mn3}S_{Mn4} + S_{Mn4}S_{Mn5} \\ +S_{Mn5}S_{Mn6} + S_{Mn6}S_{Mn7} + S_{Mn2}S_{Mn7} \end{pmatrix} \end{bmatrix} \quad (1)$$

Here J is the isotropic exchange coupling constant, with S_{Mn} representing the spins of the manganese ions. In the case of compound **2**, we have employed the following exchange Hamiltonian [Eq. (2)].

$$\hat{H} = -\begin{bmatrix} 2J_1(S_{Mn1}S_{Mn2} + S_{Mn1}S_{Mn4} + S_{Mn1}S_{Mn6}) + \\ 2J_2(S_{Mn1}S_{Mn3} + S_{Mn1}S_{Mn5} + S_{Mn1}S_{Mn7}) \\ +2J_3(S_{Mn2}S_{Mn3}) + 2J_4(S_{Mn3}S_{Mn4}) + 2J_5(S_{Mn5}S_{Mn6}) + \\ 2J_6(S_{Mn2}S_{Mn7}) + 2J_7(S_{Mn4}S_{Mn5}) + 2J_8(S_{Mn6}S_{Mn7}) \end{bmatrix} \quad (2)$$

The manganese ions in compounds **3** and **4** are labelled as shown in Figure 2. The following exchange Hamiltonian has been employed to evaluate the exchange J values in these complexes [Eq. (3)].

$$\hat{H} = -\begin{bmatrix} 2J_1\begin{pmatrix} S_{Mn1}S_{Mn2} + S_{Mn1}S_{Mn3} + S_{Mn1}S_{Mn4} \\ +S_{Mn1}S_{Mn5} + S_{Mn1}S_{Mn6} + S_{Mn1}S_{Mn7} \end{pmatrix} \\ +2J_2\begin{pmatrix} S_{Mn2}S_{Mn3} + S_{Mn3}S_{Mn4} + S_{Mn4}S_{Mn5} \\ +S_{Mn5}S_{Mn6} + S_{Mn6}S_{Mn7} + S_{Mn2}S_{Mn7} \end{pmatrix} \end{bmatrix} \quad (3)$$

The energies of five spin configurations for compound **1**, ten spin configurations for compound **2** and three spin configurations for compounds **3** and **4** are computed to extract the exchange interactions[21] (see the Supporting Information for details). The computed spin configurations for compounds **1**–**4** are given in Tables ST1–ST3 in the Supporting Information. The exchange coupling constants have been calculated by using the broken symmetry (BS) approach developed by Noodleman.[22] This method has been employed previously to compute good numerical estimates of the exchange interactions in numerous polynuclear complexes.[23] Further to the calculations on the full structure, calculations have also been performed by using the diamagnetic substitution method (DSM), where, except for the desired pair of paramagnetic metals, the remaining ions are substituted by diamagnetic cations such as Zn^{II}, Co^{III} and Ti^{IV}.[24] These calculations are necessary to gauge the J values computed from the full structure and to understand the influence that other paramagnetic metal ions have on a particular J value. Besides isotropic exchange, double-exchange mechanisms have been reported for mixed-valence complexes,[25] however we do not expect such interactions in these clusters. See Table ST4 in the Supporting Information for the computed spin-contamination values.

To analyse and comprehend the computed J values for the various Mn^{n+}–Mn^{m+} pairs even further (where n and m are 2, 3 and 4), calculations have been performed on dinuclear models and magneto–structural correlations have been developed for these pairs (see Figure SF3 and SF4 in the Supporting Information for the modelled dinuclear complexes). Because several pair wise models, with varying oxidation sates and bridging groups are detected for compounds **1**–**4**, we have used M*xy*A, M*xy*B and M*xy*C notations to classify each modelled dimer. M simply denotes model, x and y are numbers denoting the oxidation state of the two Mn ions, and A, B and C characters, which denote the various bridging ligands studied. The notation A, B and C represent $\{Mn_2(OMe)_2\}$, $\{Mn_2F(OMe)\}$ and $\{Mn_2F\}$ bridging motifs, respectively. Here all the DFT calculations were performed by using the B3LYP functional[26] with the triple-ζ-quality basis set of Ahlrich et al.[27] and all the calculations have been performed within the Gaussian 09 suite of programs.[28] The PHI[29] program was used for the simulation of the magnetic susceptibilities.

Besides the magnetic coupling, the ZFS parameters have also been computed for complex **1** by using the Orca programme suite.[30] In our DFT calculations, the spin–orbit coupling operators are represented by an effective one electron, using the spin–orbit mean-field (SOMF) method as implemented in Orca.[30] We have used the coupled perturbed (CP) SOC approach to evaluate the spin–orbit contribution to D (D_{SOC}). The spin–spin contribution (D_{SS}) was estimated by using the unrestricted natural orbital[7g] approach. To improve the accuracy of the estimated D values, relativistic corrections are performed by using the DKH method.[30] Although ab-initio CASSCF/PT2 calculations have proven to yield an accurate estimate of the D values[9c,31] this method cannot be employed for such large clusters. DFT calculations yielded electronic configuration for the Mn atoms, which are given in Table ST5 in the Supporting Information.

Experimental Section

Complexes **2** and **4** were synthesised as per literature reports.[19,20]

Magnetic measurements: Magnetic measurements were carried out on a Quantum Design SQUID magnetometer MPMS-XL7 operating between 1.8 and 300 K for dc-applied fields ranging from 0–5 T. Microcrystalline samples were dispersed in vaseline in order to avoid torquing of the crystallites. The sample mulls were contained in a calibrated gelatine capsule held at the centre of a drinking straw that was fixed at the end of the sample rod.

Results and Discussions

Selected structural parameters, which are likely to affect the magnetic properties of complexes **1**–**4** are summarised in Tables 1 and ST6–ST9 in the Supporting Information. In complex **1** the central Mn^{II} ion is surrounded by a ring of three Mn^{II} and three Mn^{IV} ions in an alternating arrangement (see Figure 1 a).[19] Experimental magnetic susceptibility measurements reveal dominant ferromagnetic exchange interactions, with a low-temperature $\chi_M T$ value suggesting a spin ground state of $S = 23/2$. For complex **2** the central Mn^{II} ion is surrounded by three Mn^{III} and three Mn^{II} ions in the outer ring. The thermal dependence of the $\chi_M T$ product for **2** suggests dominant antiferromagnetic interactions with a spin ground state of $S = 4$.[19] For complexes **3** and **4**, all Mn sites are found to be Mn^{II}. In these cases, the $\chi_M T$ versus T plots predict dominant antiferromagnetic exchange interactions, with a spin ground state predicted to be $S = 5/2$ for both complexes.[20] Fits of the experimental susceptibility data were performed for **1**, **3** and **4**, with the exchange values (J) found given in Table 2. Fitting of the experimental susceptibility data for **2** was not possible due to the large size and low symmetry of the complex.

Calculation of the magnetic exchange interactions (J)

The DFT-computed J values for complexes **1**–**4** are given in Table 2. An excellent agreement with the experimental J values

Table 1. Description of the bridging ligands and the average Mn···Mn distances between each pair wise interaction for complexes **1**–**4**.

	1		2		3		4	
J_x	Bridging ligands	d(Mn–Mn) [Å]	Bridging ligands	d(Mn–Mn) [Å]	Bridging ligands	d(Mn–Mn) [Å]	Bridging ligands	d(Mn–Mn) [Å]
J_1	μ_3-O{tea^{3-}} μ_3-O{peolH^{3-}}	3.204	μ_3-O{tea^{3-}}, μ_3-F	3.583, 3.552, 3.501	μ_3-OH μ_3-O{tea^{3-}}	3.454	$(\mu_3\text{-OMe})_2$	3.303
J_2	μ_3-O{tea^{3-}} μ_3-O{peolH^{3-}}	3.423	μ_3-F μ_3-O{teaH^{2-}} μ_3-O{tea^{3-}}	3.357, 3.355, 3.551	μ_3-OH, μ_3-O{tea^{3-}} μ_3-O{pppdH}	3.332	μ_3-OMe, μ_3-Opaa	3.304
J_3	μ_3-O{tea^{3-}} μ_3-O{peolH^{3-}} μ_3-O{teaH^{2-}} μ_3-O{teaH^{2-}}	3.271, 3.258	μ_3-F	3.897				
J_4			μ_3-O{tea^{3-}}, μ_3-O{teaH^{2-}}	3.165				
J_5			μ_3-O{tea^{3-}}, μ_3-O{teaH$_2^-$}	3.223				
J_6			μ_3-O{tea^{3-}}, μ_3-O{teaH$_2^-$}	3.251				
J_7			μ_3-F μ_3-O{piv}	3.609				
J_8			μ_2-F μ_3-O{teaH^{2-}}	3.042				

Table 2. DFT-calculated and experimental exchange coupling constants for complexes **1**–**4**.

J_x	J_{exp} [cm^{-1}]			J_{DFT} [cm^{-1}]							
				Full cluster				Dinuclear models		Diamagnetic substitution method (DSM)	
	1	3	4	1	2	3	4	1	2	1	2
J_1	−0.35	−0.1	−0.78	−0.09	−0.94	−0.55	−0.5	−0.22	−1.03	−0.21	−2.38
J_2	0.21	−0.53	−0.81	1.69	1.38	−1.04	−1.09	14.3	0.37	3.32	−0.29
J_3	1.75	–	–	0.65	−3.07	–	–	3.14	−3.65	−0.58	−6.81
J_4	–	–	–	–	2.29	–	–	–	4.70	–	15.26
J_5	–	–	–	–	4.19	–	–	–	−1.22	–	1.27
J_6	–	–	–	–	1.59	–	–	–	0.91	–	2.58
J_7	–	–	–	–	−2.35	–	–	–	−1.06	–	−8.94
J_8	–	–	–	–	0.14	–	–	–	5.27	–	1.36

was found for complexes **1**, **3** and **4**. The exchange topology used for the computational simulations for **1** and **2** are shown in Figures 1c and d, respectively, whereas the topology used for **3** and **4** is given in Figure 2c.

For complex **1**, the J_1 interaction describes the exchange between the central Mn^{II} ion with the outer-ring Mn^{IV} ions. The J_2 interaction describes the coupling between the central and the terminal Mn^{II} ions, whereas the J_3 interaction describes the coupling between the outer-ring Mn^{II} and Mn^{IV} ions. Both the DFT-calculated and the experimentally fitted parameters predict the J_2 and J_3 interactions to be ferromagnetic (F), whereas the J_1 interaction is predicted to be antiferromagnetic (AF). Although the signs are reproduced in all three cases, the magnitude of the values for J_2 and J_3 are reversed for theory and experiment. Confidence in the DFT-computed values are provided, however, by the excellent fit to both the susceptibility and the magnetisation data (see Figures 3a and 4).

In complex **2**, the J_1 interaction illustrates the coupling between the central Mn^{II} ion with the terminal Mn^{II} ions. The J_2 interaction describes the exchange between the central Mn^{II} and the ring Mn^{III} ions. J_3–J_6 interactions describe the coupling between the outer-ring Mn^{II} and Mn^{III} ions. The J_7 interaction describes the coupling between two outer-ring Mn^{II} ions and the J_8 interaction describes the exchange between two outer-ring Mn^{III} ions. Calculations yield strong AF interactions for J_1, J_3 and J_7, whereas J_2, J_4, J_5 and J_6 are calculated to be ferromagnetic in nature. The J_8 interaction is computed to be weakly ferromagnetic. Simulation of the magnetic susceptibility data by using the computed DFT J values for complex **2** yielded a less than satisfactory fit to the experimental data.

Because all three computational methods yielded similar sets of J values, we decided to see if there was any issues with the experimental data, such as ageing/oxidation of the sample, which can be common in transition-metal cluster chemistry.[24b,32] We therefore re-synthesised **2**, and re-measured the susceptibility and magnetisation data. The fresh sample yielded an improved fit to the DFT-simulated magnetic data (see Figures 3b and SF1 in the Supporting Information), which likely suggests that there was an ageing problem with the earlier reported sample.[19] This highlights an important issue pertaining to this chemistry and to re-iterate the need for more than one set of tools (experimental or theoretical) to obtain a reliable set of spin Hamiltonian parameters. We still note, however, that although the agreement between the experiment and theory is better on the fresh sample, below 50 K, some deviations are noted. This may be attributed to the magnetic anisotropy of the Mn^{III} ions or intermolecular interactions, which are strong in the case of complex **2** as noted earlier.[19]

For complexes **3** and **4**, the J_1 interaction describes the coupling between the central and the terminal Mn^{II} ions, whereas the J_2 interaction describes the coupling between the two outer-ring Mn^{II} ions. For complex **3** the DFT-simulated and the

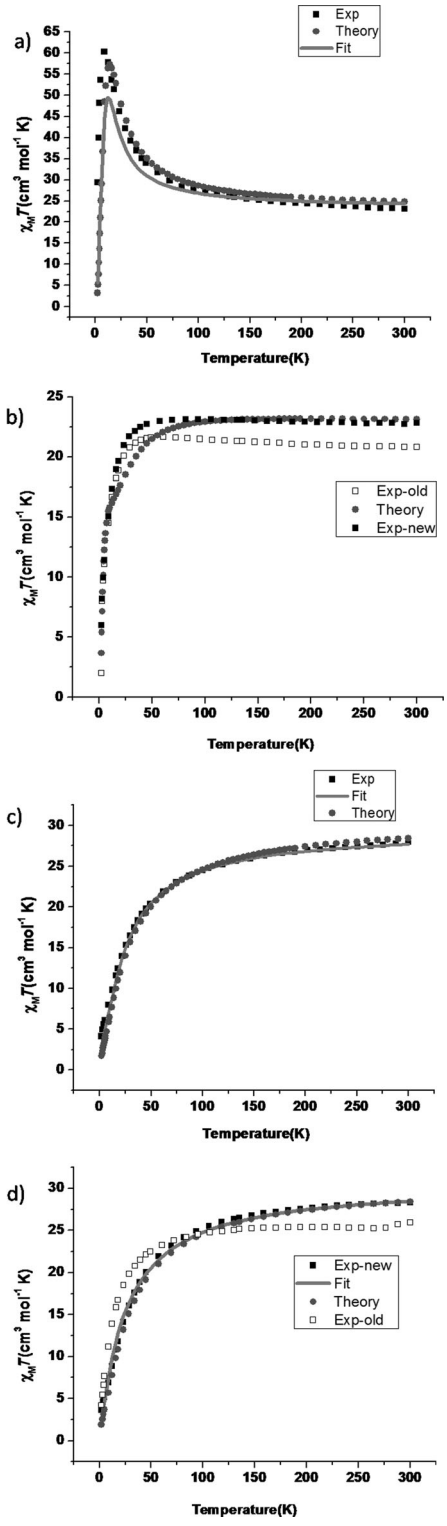

Figure 3. Thermal variation of $\chi_M T$ for a) complex **1**, b) complex **2**, c) complex **3** and d) complex **4** from 300 to 2 K under a magnetic field of 1 T.

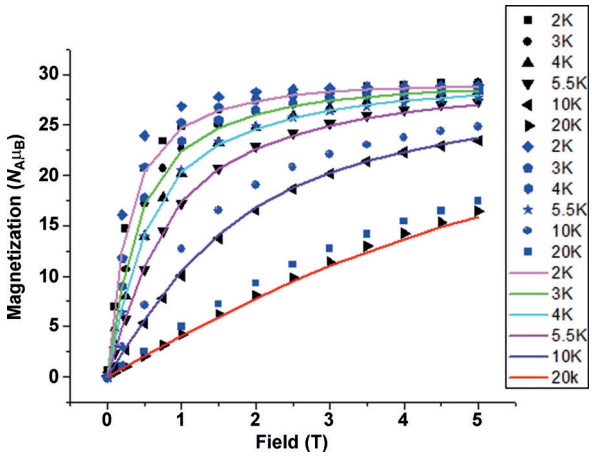

Figure 4. Plots of *M* versus *H* isotherms for complex **1** at 2 , 3, 4, 5.5, 10 and 20 K. The black shapes are experimental data, the blue shapes represent the simulation with DFT values and the colour lines are fits of the experimental data.

experimentally fitted values predict that both the J_1 and J_2 interactions are antiferromagnetic in nature (see Table 2), although the strength of the computed *J* values are slightly different than the reported experimental fits. Simulation of the magnetic data with the computed exchange constants reproduces the experimental magnetic data very well (see Figures 3c and SF2a in the Supporting Information). Although a small discrepancy in magnitude was found, we note that it is the ratio of J_1/J_2, rather than the magnitude of the interaction that significantly influences the magnetic behaviour (see Figures SF6 and SF7 in the Supporting Information).

For complex **4** both the *J* values are computed to be antiferromagnetic and consistent with the sign of the experimentally fitted values. The simulated magnetic data derived from the DFT parameters, however, did not perfectly reproduce the experimental points (see Figures 3d and SF2b in the Supporting Information). We again looked at the possibility of sample degradation/ageing and re-synthesised **4**. The susceptibility measurement on the fresh sample now revealed a striking match to the computed simulated curve.

Correlation to experiment and spin density analysis:

The dominant interaction predicted for complex **1** is the ferromagnetic J_2 interaction, leading to a spin-up configuration on the central and the outer-ring Mn^{II} ions. The next strongest interaction is the Mn^{II}···Mn^{IV} J_3 pathway, which is also ferromagnetic, leading to a spin-up configuration on all the Mn^{IV} centres. The J_1 interaction is antiferromagnetic and is competing with both the J_2 and J_3 interactions, however, this interaction is extremely weak, leading overall to an $S=29/2$ ground state for complex **1** (see Figure 1b and see Figure 6a). This is the maximum spin value achievable for this system. The experimental magnetisation saturation value of 29 $N\mu_B$ at 2 K also reveals a $S=29/2$ spin ground state (see Figure 4),[19] which is in agreement with the ground state computed by using the DFT-calculated *J* values. Several excited states with smaller *S* values are found to lie close to the ground state (see Figure 5a). The computed spin-density plot of the $S=29/2$ ground state is shown in Figure 6a. All the Mn^{II} ions present possess spin densities of <5.0, with the central Mn^{II} ion displaying a lower spin-density value than the outer-ring sites. The bridging μ_3-O

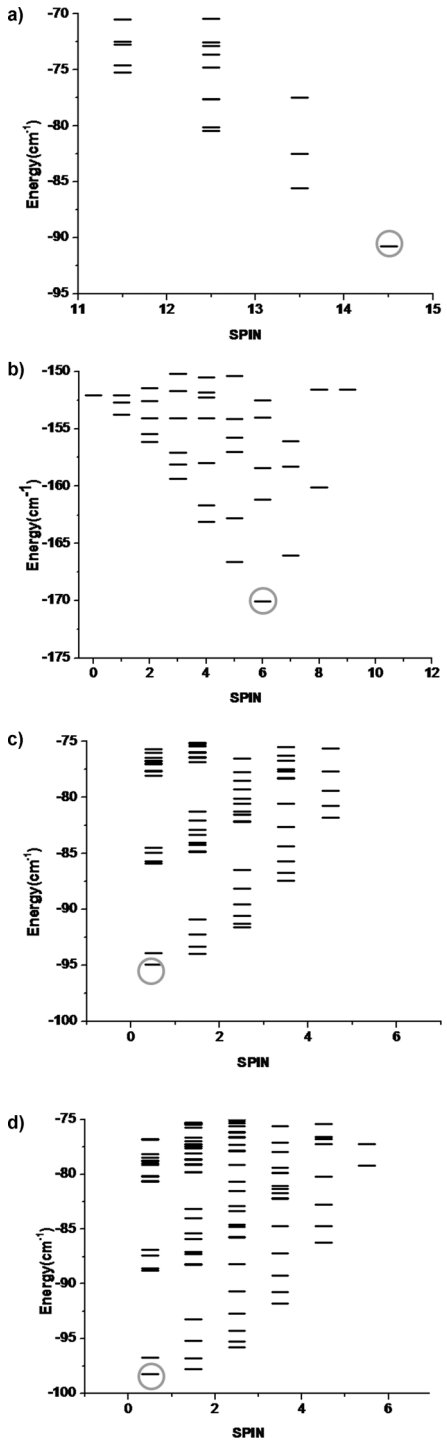

Figure 5. Computed energy levels showing the lowest lying magnetic states up to 25 cm^{-1} from the ground state for a) complex **1**, b) complex **2**, c) complex **3** and d) complex **4**. The ground states are highlighted in circles with values of {**1**, $S=29/2$}, {**2**, $S=6$}, {**3**, $S={}^{1}/_{2}$} and {**4**, $S={}^{1}/_{2}$}. The full energy spectrum for these complexes is given in Figure SF5 in the Supporting Information.

atoms from the tea^{3-} group gain a spin density of approximately 0.01 in magnitude and a major part of this density is expected to be gained from the Mn^{II} ions through spin delocalisation. All the Mn^{IV} ions have a spin-density value of >3.0 indicating dominant spin polarisation. Although complex **1** possesses a very large spin ground state, it does not display any slow relaxation of the magnetisation, even at very low temperatures. We computed the value of D to probe the reason(s) for the absence of SMM behaviour. The DFT calculations yielded a positive sign of D, with a value of $D=+0.0182\ cm^{-1}$ and $E/D=0.0035$. The magnitude and the sign are not surprising as neither Mn^{II} nor Mn^{IV} ions possess significant single-ion anisotropy. This is affirmed in our analysis where the major contribution to D is found to arise from the spin–spin contribution ($D_{ss}=0.0172\ cm^{-1}$).

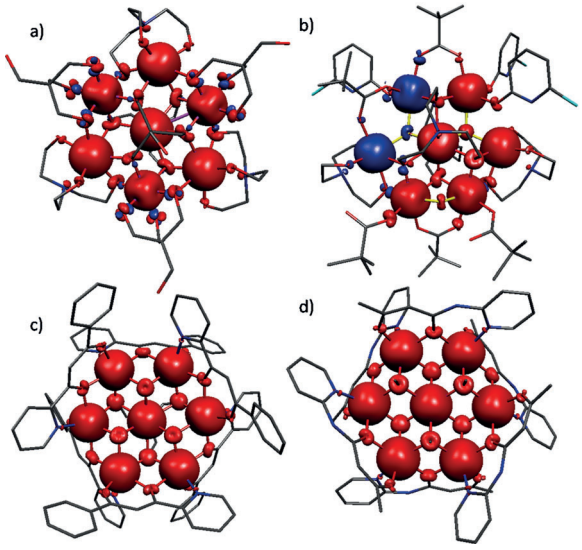

Figure 6. DFT-computed spin-density plots of a) complex **1**, b) complex **2**, c) complex **3** and d) complex **4**. The red and blue colours represent positive and negative spin densities, respectively.

For complex **2**, the DFT-computed J values yielded an $S=6$ ground state (see Figure 5b), whereas the low-temperature experimental $\chi_M T$ data suggest a ground state of $S=3$ or 4. The expected ground-state spin configuration based on the J values for a simple spin "up", spin "down" picture would yield an $S=7$ value (see Figure 1d), however, competing interactions within the structure leads to an $S=6$ ground state. The DFT-computed spin-density plot for **2** is shown in Figure 6b. The Mn^{II} ions propagate the spin densities through spin delocalisation, similar to **1**, whereas the Mn^{III} ions exhibit a mixture of spin delocalisation and polarisation.

In complexes **3** and **4**, both the J_1 and J_2 interactions are antiferromagnetic in nature. These are of comparable magnitudes and, therefore, the competing interactions result in a ground state of $S=1/2$ (see Figures 5c and d). The experimental magnetic data were however fitted to yield a $S=5/2$ ground state.[20] The spin-state diagrams computed from DFT are shown in Figures 5c and d and show a large number of low lying excited states of value $S=1/2$, $S=5/2$ (and $S=3/2$) for both complexes, displaying the difficulty in resolving the ground state from experimental data alone, when the exchange is weak. The computed spin-density plots for the Mn^{II} ions show a dominant spin delocalisation mechanism.

Analysing the exchange interactions

Although the computed J values for complexes **1**–**4** are presented above, no rationale for the observed behaviour was discussed. We have therefore analysed the structure and determined the reasons for the sign and magnitude of the J values obtained. To probe the differences in the observed magnetic properties and to unravel whether the differences found are due to the Mn oxidation states or because of the structure, we have modelled several dinuclear complexes corresponding to different pair wise pathways (J) present. Essentially, there are seven different building units (BUs) present in **1**–**4** and the core structures of these seven dinuclear models are shown in Scheme 1 (see Figures SF3 and SF4 in the Supporting Information for model structures). The computed magnetic exchange for these BUs, along with the origin of the magnetic interaction, is presented in detail below.

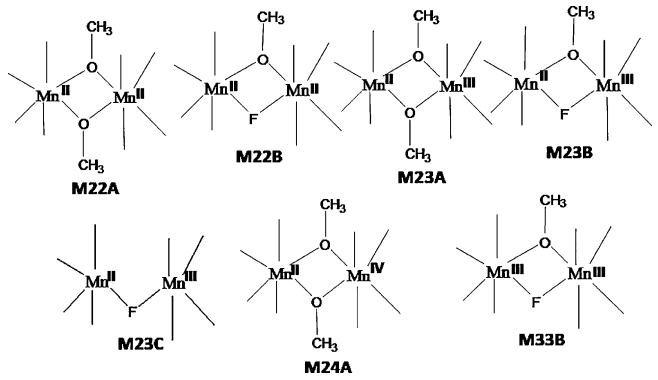

Scheme 1. Dinuclear building units present in complexes **1**–**4**. ("A" represents the $[Mn_2(OMe)_2]$ bridging unit, "B" represents the $[Mn_2F(OMe)]$ fragment and "C" the $[Mn_2F]$ fragment).

M24A model (Mn^{II}–Mn^{IV} interactions)

In complex **1**, both the J_1 and J_3 interactions correspond to $Mn^{II}\cdots Mn^{IV}$ coupling. Calculations on this BU yielded J_1 as $-0.22\ cm^{-1}$ and this estimate is similar to the J_1 value estimated in the full cluster calculation (see Table 2 and Figure SF3a in the Supporting Information for the model structure). The model not only reproduces the sign of J_1 but also the magnitude, offering confidence towards the AF interaction predicted for this pair.

To understand the nature of the coupling we have analysed the overlap integral between the singly occupied molecular orbitals (SOMOs) of the two Mn centres. Two interactions, $|d_{xz}|d_{xz}|$ and $|d_{xy}|d_{xy}|$ are found to be significant, whereas other overlaps are negligible (see Table ST10 in the Supporting Information for the overlap integral values and Figure SF8 in the Supporting Information). Here the interaction between the two d_{xy} orbitals is a through-space interaction and the metal–metal distance plays a role in controlling this interaction. The interaction between the two d_{xz} orbitals is mediated through the μ-OMe group and this is a π-type interaction. Because these two overlaps are prominent, the overall coupling is antiferromagnetic; however, it is weak in nature as other orbital interactions are essentially orthogonal. We expanded upon this and have developed magneto–structural correlations for this pair. Variations were made in the Mn–O distance, Mn-O-Mn angle and Mn-O-Mn-O dihedral angles. Among the three correlations developed (see Figures 7a and Figure SF9 in the Supporting Information) the Mn-O-Mn angle is found to significantly influence the J value compared to the other two parameters. The computed correlation is exponential in nature, with a smaller angle (less than 100°) leading to antiferromagnetic coupling and a larger angle (greater than 100°) yielding weak ferromagnetic coupling. Although a correlation for this pair has not previously been developed, correlations developed for a $Mn^{IV}\cdots Mn^{IV}$ interaction revealed a similar trend.[33]

The J_3 interaction in complex **1** also belongs to this model. The interaction is computed to be ferromagnetic ($+0.65\ cm^{-1}$) for the full cluster calculation. The computed J_3 interaction for the model dimer ($+3.14\ cm^{-1}$) is found to complement the sign of the full cluster calculation (see Figure SF3c in the Supporting Information for the structure of the model dimer). The Mn-O-Mn angles for this pair are 101 and 103° and our developed correlation predicts ferromagnetic coupling of $+1.1\ cm^{-1}$, which is in excellent agreement with the calculations made on the full structure and the model dimer. Because the interaction is switched to ferromagnetic compared to J_1, due to the larger angles, we went on to analyse the magnetic orbitals. It was found that the $|d_{xz}|d_{xz}|$ and $|d_{xy}|d_{xy}|$ overlaps are negligible. As the Mn-O-Mn angle expands, the π-type interaction through the d_{xz} orbital weakens and the larger Mn–Mn distance nullifies the $|d_{xy}|d_{xy}|$ interaction, leading to the weak ferromagnetic coupling for this pair (see Table ST11 in the Supporting Information).

M22A model (Mn^{II}–Mn^{II} interaction)

In complex **1** the J_2 interaction belongs to this class. The developed dimer model yields a ferromagnetic J consistent with the calculation on the full structure, however, the magnitude is overestimated: $+14.3$ versus $+1.69\ cm^{-1}$ (see Figure SF3b in the Supporting Information for the structure of the model dimer). Analysing the origin of the exchange reveals no significant SOMO–SOMO interaction (see Table ST12 in the Supporting Information) resulting in orbital orthogonality, and thus ferromagnetic coupling for this pair. Beyond **1**, the same BU is also present in complexes **3** and **4**, with the J_1 and J_2 interactions belonging to this category. In these cases, however, the interactions are computed to be AF in nature. To rationalise this observation, magneto–structural correlations were developed for this Mn^{II}–Mn^{II} pair. It was found that the Mn–O distance significantly influences the J values, whereas other structural parameters have little effect (see Figures 7b and SF10 in the Supporting Information). The correlation indicates that long and short Mn–O bond lengths yield antiferromagnetic exchange, which is consistent with the structural parameters observed for the Mn^{II}-$(OMe)_2$-Mn^{II} pairs in **3** and **4** (see Tables 1 as well as ST8 and ST9 in the Supporting Information).

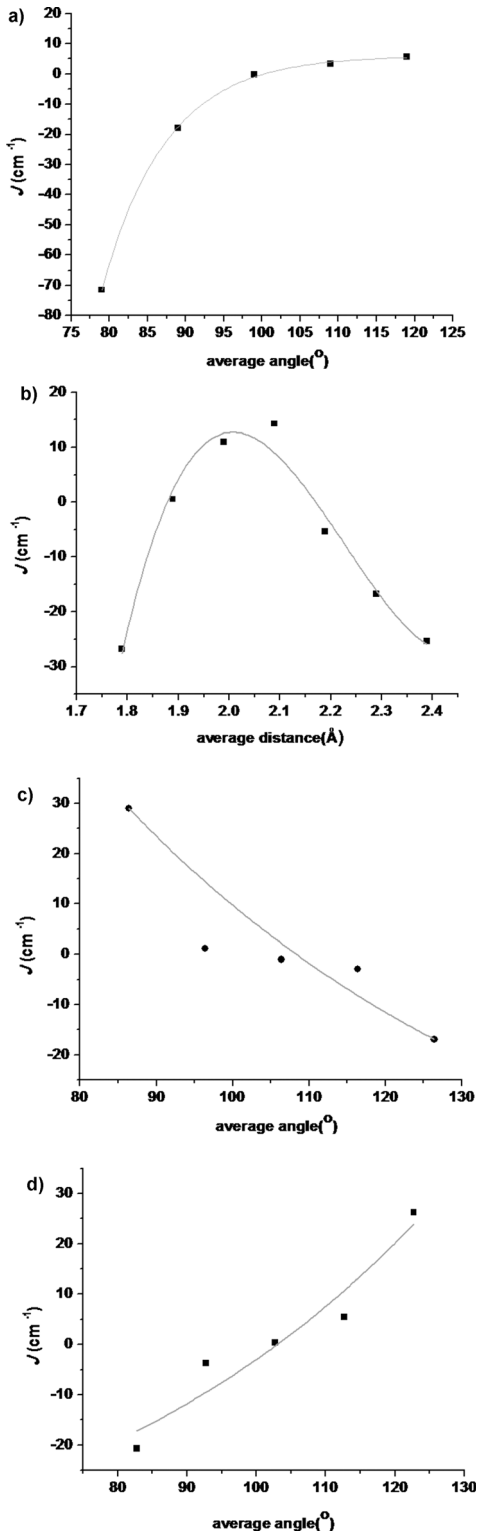

Figure 7. Magneto–structural correlation developed for a) the Mn-O-Mn angle in the M24A BU, b) the average Mn–O distance in the M22A BU, c) the average angle in the M22B BU and d) the average angle in the M23B BU.

M22B model (Mn^{II}–Mn^{II} interactions)

In complex **2** the J_1 and J_7 exchange pathways corresponds to this BU. The modelled dimer (see Figure SF4a in the Supporting Information) yielded an antiferromagnetic interaction ($-1.03\ cm^{-1}$) similar to the corresponding J values in the full structure calculation. Here the $|d_{xy}|d_{yz}|$ and $|d_{xz}|d_{xz}|$ SOMO interactions are found to be significant, whereas other overlaps are negligible (see Table ST13 and Figure SF11 in the Supporting Information). This overlap is essentially super-exchange in nature and contributes to the antiferromagnetic part of the net exchange. Here, the correlation developed for the average angle (see Figures 7c and SF12 in the Supporting Information) is found to significantly influence the J values, compared to the average distance and the Mn-F-Mn-O dihedral angle parameters, which have little effect on the exchange. The developed correlation reveals that angles greater than 105° result in antiferromagnetic coupling, whereas angles less than 105° lead to ferromagnetic exchange. The J_7 interaction in complex **2** has an average Mn-O-Mn angle of 105.6° (see Table ST7b in the Supporting Information) and our developed correlation predicted an antiferromagnetic interaction for this pair, which is in agreement with the computed J value determined from the full structure calculation.

M23B model (Mn^{II}–Mn^{III} interactions)

The J_2 interaction in complex **2** corresponds to this BU. The calculated J on the BU reproduces the ferromagnetic coupling observed on the full structure ($0.37\ cm^{-1}$). Because no significant SOMO–SOMO overlap is detected, the coupling is ferromagnetic for this pair (see Table ST14 in the Supporting Information). As mentioned in earlier models the average angle was found to play a pivotal role in influencing the J values. This is found to be the case here, with an angle greater than 102° favouring ferromagnetic exchange, and an angle less than 102° favouring antiferromagnetic coupling (see Figure 7d and SF13 in the Supporting Information). This trend is contrary to our earlier observation for the Mn^{II}–Mn^{II} pair (M22B). The $d_{x^2-y^2}$ orbital is not occupied at the Mn^{III} centre and, due to the strong orthogonality between the two $d_{x^2-y^2}$ orbitals, a significant ferromagnetic contribution is observed at higher angles. At lower angles this interaction leads to AF coupling.

M23C (Mn^{II}–Mn^{III} interactions)

The J_3 interaction in complex **2** corresponds to this BU. Calculations for the dinuclear model resulted in a J value of -6.81 compared to $-3.07\ cm^{-1}$ for the full structure. Here the $|d_{xz}|d_{z^2}|$ overlap (see Figure SF14 and Table ST15 in the Supporting Information) between the two SOMOs is found to be significant leading to an AF interaction. Both the Mn–F distance and Mn-F-Mn angles are found to be important. The smaller the Mn-F-Mn angle (an angle less than 120° results in a sharp decrease and a larger AF contribution) and the shorter the Mn–F bond length (less than 2.2 Å results in a sharp decrease and a larger AF contribution) increase the antiferromagnetic exchange further (see Figures 8a and b and Table ST7b in the Supporting Information).

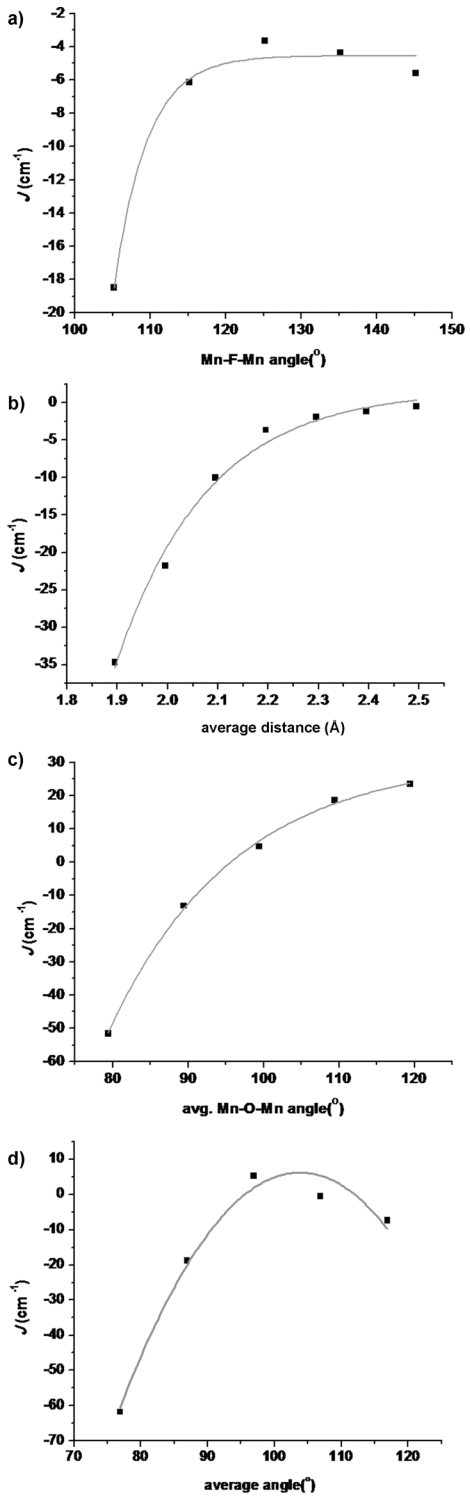

Figure 8. Magneto–structural correlations developed for a) the average Mn-F-Mn angle for the M23C BU, b) the average Mn–F distance in the M23C BU, c) the average Mn-O-Mn angle for the M23A BU and d) the average angle for the M33B BU.

M23A *model (Mn^{II}–Mn^{III} interactions)*

The J_4, J_5 and J_6 interactions in complex **2** corresponds to this BU. Calculations for J_4 by using the dinuclear model yielded ferromagnetic exchange (4.70 cm^{-1}), which is similar to the full cluster estimate (see Table 2). The magnetic orbitals are essentially orthogonal and the lack of SOMO–SOMO interaction for this model (see Table ST16 in the Supporting Information) results in weak ferromagnetic coupling for this pair. The developed correlation suggests that the average Mn-O-Mn angle plays an important role in determining the strength of J (see Figures 8c and SF15 in the Supporting Information). It was found that at angles greater than 95° the interaction is ferromagnetic, whereas it is antiferromagnetic below this angle. The trend found is similar to the earlier Mn^{II}–Mn^{III} model (M23B) where a larger angle (>102°) resulted in ferromagnetic coupling, whereas an angle below 102° yielded an AF interaction. This result is supported by pressure studies performed on a Mn^{II}–Mn^{III}–Mn^{II} SMM, where larger pressures lead to smaller angles and therefore a reduction in the ferromagnetic coupling.[34]

The average Mn-O-Mn angles for J_5 and J_6 correspond to 100.7 and 102.3°, respectively. Our developed correlation correctly predicts ferromagnetic coupling for these angles (+8.2 and +10.2 cm^{-1} for J_5 and J_6, respectively), which is in agreement with the value calculated for the full structure—however the magnitude of J is overestimated.

M33B *model (Mn^{III}–Mn^{III} interaction)*

The J_8 interaction in complex **2** corresponds to this BU. The dinuclear model (see Figure SF4h in the Supporting Information) yields a ferromagnetic J value of 5.27 cm^{-1} consistent with the full structure calculation. The large Mn-F-Mn angle (104.5°) (see also Table ST7b in the Supporting Information) and the Mn-O-Mn angle of approximately 90° (89.5°) leads to net ferromagnetic exchange and strict orbital orthogonality between the SOMOs are witnessed (see Table ST17 in the Supporting Information). The correlation developed for the average Mn-O-Mn and Mn-F-Mn angles is shown in Figure 8d (also refer to Figure SF16 in the Supporting Information for the correlation developed for other structural parameters). Here an angle of >95° yields a ferromagnetic interaction, whereas angles below this result in a strong AF interaction. A maximum ferromagnetic interaction is observed around 102°, before becoming antiferromagnetic again above 110°.

Discussion of the devised correlations

In the preceding section we have discussed the individual magneto–structural correlations relating to the effect the bond angle has on J. In Figure 9c we have combined the correlations into a single plot. The plot reveals that the influence of the bond angle is difficult to predict and it strongly correlates to the nature of the bridge and the angle parameter. Some commonality can, however, be derived (M22B model excluded), where all the structures yield AF interactions at lower Mn-O/F-Mn angles and weak antiferromagnetic to moderate ferromagnetic interaction at larger angles. Except for model M23C, the angle can be utilised to switch the interaction from ferro- to antiferromagnetic and vice versa. Furthermore, independent of the Mn oxidation state or the nature of the bridging group,

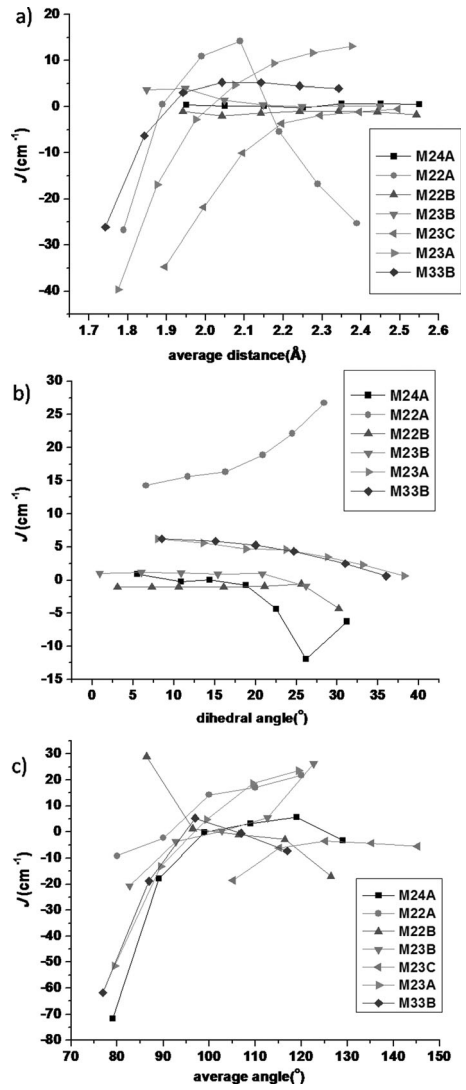

Figure 9. Magneto–structural correlation for a) the average Mn–O/Mn–F distances, b) the Mn-O-Mn-O/Mn-F-Mn-O dihedral angles and c) the average Mn-O-Mn/Mn-F-Mn bridging angle corresponding to all the BUs.

a larger variation in the value of *J* is observed upon varying the angle parameter in all cases. This suggests that the magnetic properties of manganese clusters can be manipulated easily by changing the bond angle parameter alone.

Correlations developed for Mn–O/Mn–F distances and Mn-O-Mn-O/Mn-F-Mn-O dihedral angles to check for common trends are shown in Figures 9a and b, respectively. The distance correlation, except for model M22A, reveals a general trend, where the magnetic interactions are either weakly ferromagnetic or close to zero at long Mn–O/Mn–F distances, whereas the shorter Mn–O/Mn–F distances yield AF interactions. This can be connected with the fact that longer Mn–O/Mn–F distances lead to a weaker interaction between the SOMOs resulting in zero or weak ferromagnetic coupling. Short distances promote a strong orbital overlap and therefore antiferromagnetic interactions are observed. For the M22A model, strong AF interactions are noted even at Mn–O distance of 2.4 Å and this may be due to a very strong σ overlap between the SOMOs propagating through the two methoxide bridges. Interestingly, for models M22B, M24B and M23B, no significant change in the *J* values was observed upon variation in the Mn–O/Mn–F distances. For the Mn-O-Mn-O/Mn-F-Mn-O dihedral angle correlations (see Figure 9b) only minimal changes in the *J* values are observed, with larger dihedral angles leading to an increasing contribution to the antiferromagnetic component of the exchange. Model M22A is again an exception, with the opposite behaviour noted.

Conclusion

Four structurally similar hetero- and homo-valent heptanuclear disc-like $\{Mn_7\}$ clusters were modelled by using density functional methods with the key aim being the computation of the magnetic exchange pathways and to probe the origin of the magnetic exchange present in the pair-wise building units present in the clusters. The conclusions derived from this work are summarised below.

1) The computational method B3LYP/TZV was found to yield good numerical estimates of the exchange constants (*J*) for all four complexes studied despite the fact the exchange constants in these clusters are numerically very small.
2) The magnetic susceptibility data computed by using the DFT-calculated *J* values are in remarkably good agreement with experimental $\chi_M T$ versus *T* data. Even minor variations observed for complexes **2** and **4**, in earlier reported data[19,20] were found to fall in line with the DFT-simulated curve once the data had been re-measured on a fresh sample. This clearly suggests that more than one experimental method, that is, SQUID susceptibilities, inelastic neutron scattering (INS) and EPR in conjunction with each other, or by other independent methods, are required to verify the experimental data and to extract a reliable set of spin Hamiltonian parameters in polynuclear spin-coupled clusters. Inputs from computational methods, such as the one described here, are mandatory for larger clusters possessing several exchange constants.
3) Among the present complexes, only complex **1** possesses a very large and relatively isolated ground state. This is due to the structural topology of alternating Mn^{II} and Mn^{IV} ions. A similar Mn^{II} and Mn^{III} pair arrangement, reported by others, also yielded similarly large spin ground state values.[10a–c] The isostructural homo-valent Mn^{II} and hetero-valent $\{Mn^{II}Mn^{III}\}$ clusters **2**–**4** reported here possess smaller spin ground state values. This highlights the importance of the oxidation states and their position (topology) in polynuclear clusters in order to obtain a large and isolated spin ground state.[10a,b,35]
4) Seven unique BU structures are detected within these large clusters, and control the overall magnetic susceptibility behaviour. There are three sub-types of BUs, which can be categorised by the bridging ligands between the metal ions. The first class possesses two methoxide bridges (A), whereas the second possesses one methoxide and one fluoride bridge (B) (the third describes a single F bridge

(C)). Interestingly, as we go from M22A to M23A and M24A (22 for example denotes a Mn^{II}–Mn^{II} interaction), the ferromagnetic contribution to *J* decreases and the interaction becomes weakly antiferromagnetic, as we progress with the oxidation of the metal ions. This is due to the loss of $|d_{x^2-y^2}|d_{x^2-y^2}|$ orbital contributions to the ferromagnetic part of *J* as the Mn ion gets oxidised.

5) A reverse trend to point 4 is visible if we go from M22B to M23B and M33B and illustrates the role of the bridging fluoride ion in switching the magnetic coupling in these clusters. The fluoride ion promotes stronger delocalisation of the spins and possesses relatively wider angles compared to the methoxide oxygen-atom bridges, leading to a reversal of the trend observed with the bis methoxide models.
6) The extensive magneto–structural correlations developed reveal, overall, that the major factor controlling the magnetic exchange lies with the Mn-O-Mn/Mn-F-Mn angle, for all the pairs studied, independent of the nature of the bridging group. This suggests that the magnetic properties of large polynuclear can be fine-tuned by adjusting the angle parameter.

In summary, the theoretical study undertaken here has unlocked some important aspects of the magnetic properties of large polynuclear complexes, such as how ageing in polynuclear Mn clusters affects the magnetism and fitting from the originally devised structure. This suggests that a theoretical approach, in conjunction with experimental methods is needed to unequivocally determine the spin Hamiltonian parameters of the complex. The magneto–structural correlations established here have wide scope beyond the examples presented and we are currently testing this in other Mn clusters.

Acknowledgements

G.R. would like to acknowledge the financial support from DST India, and IIT Bombay for the high performance computing facility. K.R.V. is thankful to the IITB-Monash Research Academy for a PhD studentship. G.R. and K.S.M. acknowledge the support of an Australia-India Strategic Research Fund (AISRF) grant.

Keywords: cluster compounds · density functional calculations · magnetic properties · manganese · oxidations states

[1] R. Sessoli, D. Gatteschi, A. Caneschi, M. A. Novak, *Nature* **1993**, *365*, 141 – 143.
[2] a) G. Christou, D. Gatteschi, D. N. Hendrickson, R. Sessoli, *MRS Bull.* **2000**, *25*, 66 – 71; b) R. S. D. Gatteschi, J. Villain, *Molecular Nanomagnets*, Oxford University Press, Oxford, **2006**.
[3] a) R. Sessoli, H. L. Tsai, A. R. Schake, S. Wang, J. B. Vincent, K. Folting, D. Gatteschi, G. Christou, D. N. Hendrickson, *J. Am. Chem. Soc.* **1993**, *115*, 1804 – 1816; b) N. E. Chakov, S.-C. Lee, A. G. Harter, P. L. Kuhns, A. P. Reyes, S. O. Hill, N. S. Dalal, W. Wernsdorfer, K. A. Abboud, G. Christou, *J. Am. Chem. Soc.* **2006**, *128*, 6975 – 6989.
[4] a) C. J. Milios, A. Vinslava, W. Wernsdorfer, A. Prescimone, P. A. Wood, S. Parsons, S. P. Perlepes, G. Christou, E. K. Brechin, *J. Am. Chem. Soc.* **2007**, *129*, 6547 – 6561; b) C. J. Milios, R. Inglis, A. Vinslava, R. Bagai, W. Wernsdorfer, S. Parsons, S. P. Perlepes, G. Christou, E. K. Brechin, *J. Am. Chem. Soc.* **2007**, *129*, 12505 – 12511; c) C. J. Milios, A. Vinslava, W. Wernsdorfer, S. Moggach, S. Parsons, S. P. Perlepes, G. Christou, E. K. Brechin, *J. Am. Chem. Soc.* **2007**, *129*, 2754 – 2755.
[5] a) N. Ishikawa, M. Sugita, T. Ishikawa, S. Koshihara, Y. Kaizu, *J. Am. Chem. Soc.* **2003**, *125*, 8694 – 8695; b) N. Ishikawa, M. Sugita, W. Wernsdorfer, *Angew. Chem.* **2005**, *117*, 2991 – 2995; *Angew. Chem. Int. Ed.* **2005**, *44*, 2931 – 2935; c) M. Waters, F. Moro, I. Krivokapic, J. McMaster, J. van Slageren, *Dalton Trans.* **2012**, *41*, 1128 – 1130; d) J. D. Rinehart, M. Fang, W. J. Evans, J. R. Long, *Nat. Chem.* **2011**, *3*, 538 – 542; e) J. D. Rinehart, M. Fang, W. J. Evans, J. R. Long, *J. Am. Chem. Soc.* **2011**, *133*, 14236 – 14239; f) M. Nematirad, W. J. Gee, S. K. Langley, N. F. Chilton, B. Moubaraki, K. S. Murray, S. R. Batten, *Dalton Trans.* **2012**, *41*, 13711 – 13715; g) S. K. Langley, N. F. Chilton, I. A. Gass, B. Moubaraki, K. S. Murray, *Dalton Trans.* **2011**, *40*, 12656 – 12659; h) S. Demir, J. M. Zadrozny, M. Nippe, J. R. Long, *J. Am. Chem. Soc.* **2012**, *134*, 18546 – 18549; i) Y.-N. Guo, G.-F. Xu, W. Wernsdorfer, L. Ungur, Y. Guo, J. Tang, H.-J. Zhang, L. F. Chibotaru, A. K. Powell, *J. Am. Chem. Soc.* **2011**, *133*, 11948 – 11951; j) Y.-N. Guo, G.-F. Xu, P. Gamez, L. Zhao, S.-Y. Lin, R. Deng, J. Tang, H.-J. Zhang, *J. Am. Chem. Soc.* **2010**, *132*, 8538 – 8539; k) I. J. Hewitt, Y. Lan, C. E. Anson, J. Luzon, R. Sessoli, A. K. Powell, *Chem. Commun.* **2009**, 6765 – 6767; l) Y.-L. Miao, J.-L. Liu, J.-D. Leng, Z.-J. Lin, M.-L. Tong, *CrystEngComm* **2011**, *13*, 3345 – 3348; m) J. W. Sharples, Y.-Z. Zheng, F. Tuna, E. J. L. McInnes, D. Collison, *Chem. Commun.* **2011**, *47*, 7650 – 7652; n) S. K. Langley, B. Moubaraki, K. S. Murray, *Inorg. Chem.* **2012**, *51*, 3947 – 3949.
[6] a) A. M. Ako, I. J. Hewitt, V. Mereacre, R. Clérac, W. Wernsdorfer, C. E. Anson, A. K. Powell, *Angew. Chem.* **2006**, *118*, 5048 – 5051; *Angew. Chem. Int. Ed.* **2006**, *45*, 4926 – 4929; b) E. Ruiz, T. Cauchy, J. Cano, R. Costa, J. Tercero, S. Alvarez, *J. Am. Chem. Soc.* **2008**, *130*, 7420 – 7426; c) R. E. P. Winpenny, *Molecular Cluster Magnets*,World Scientific Publishing, New York, **2011**.
[7] a) S. Piligkos, G. Rajaraman, M. Soler, N. Kirchner, J. van Slageren, R. Bircher, S. Parsons, H.-U. Gudel, J. Kortus, W. Wernsdorfer, G. Christou, E. K. Brechin, *J. Am. Chem. Soc.* **2005**, *127*, 5572 – 5580; b) E. Cremades, J. Cano, E. Ruiz, G. Rajaraman, C. J. Milios, E. K. Brechin, *Inorg. Chem.* **2009**, *48*, 8012 – 8019; c) E. Cremades, E. Ruiz, *Inorg. Chem.* **2010**, *49*, 9641 – 9648; d) J. E. McGrady, R. Stranger, *J. Am. Chem. Soc.* **1997**, *119*, 8512 – 8522; e) T. Krämer, Z. Lin, J. E. McGrady, *Dalton Trans.* **2011**, *40*, 927 – 932; f) H. Nagao, M. Nishino, Y. Shigeta, T. Soda, Y. Kitagawa, T. Onishi, Y. Yoshioka, K. Yamaguchi, *Coord. Chem. Rev.* **2000**, *198*, 265 – 295; g) K. Koizumi, M. Shoji, Y. Kitagawa, T. Taniguchi, T. Kawakami, M. Okumura, K. Yamaguchi, *Polyhedron* **2005**, *24*, 2720 – 2725; h) G. Rajaraman, M. Murugesu, E. C. Sanudo, M. Soler, W. Wernsdorfer, M. Helliwell, C. Muryn, J. Raftery, S. J. Teat, G. Christou, E. K. Brechin, *J. Am. Chem. Soc.* **2004**, *126*, 15445 – 15457.
[8] a) S. Piligkos, E. Bill, D. Collison, E. J. L. McInnes, G. A. Timco, H. Weihe, R. E. P. Winpenny, F. Neese, *J. Am. Chem. Soc.* **2007**, *129*, 760 – 761; b) F. Neese, E. I. Solomon, *Inorg. Chem.* **1998**, *37*, 6568 – 6582; c) L. F. Chibotaru, L. Ungur, C. Aronica, H. Elmoll, G. Pilet, D. Luneau, *J. Am. Chem. Soc.* **2008**, *130*, 12445 – 12455; d) E. Cremades, E. Ruiz, *Inorg. Chem.* **2011**, *50*, 4016 – 4020; e) S. Gómez-Coca, E. Cremades, N. Aliaga-Alcalde, E. Ruiz, *Inorg. Chem.* **2014**, *53*, 676 – 678.
[9] a) G. N. Cavigliasso, P. Comba, R. Stranger, *Inorg. Chem.* **2004**, *43*, 6734 – 6744; b) V. Barone, A. Bencini, D. Gatteschi, F. Totti, *Chem. Eur. J.* **2002**, *8*, 5019 – 5027; c) S. Sinnecker, F. Neese, L. Noodleman, W. Lubitz, *J. Am. Chem. Soc.* **2004**, *126*, 2613 – 2622.
[10] a) T. C. Stamatatos, K. M. Poole, D. Foguet-Albiol, K. A. Abboud, T. A. O'Brien, G. Christou, *Inorg. Chem.* **2008**, *47*, 6593 – 6595; b) T. C. Stamatatos, D. Foguet-Albiol, K. M. Poole, W. Wernsdorfer, K. A. Abboud, T. A. O'Brien, G. Christou, *Inorg. Chem.* **2009**, *48*, 9831 – 9845; c) M. A. Bolcar, S. M. J. Aubin, K. Folting, D. N. Hendrickson, G. Christou, *Chem. Commun.* **1997**, 1485 – 1486; d) N. C. Harden, M. A. Bolcar, W. Wernsdorfer, K. A. Abboud, W. E. Streib, G. Christou, *Inorg. Chem.* **2003**, *42*, 7067 – 7076; e) B. Pilawa, M. T. Kelemen, S. Wanka, A. Geisselmann, A. L. Barra, *Europhys. Lett.* **1998**, *43*, 7; f) R. W. Saalfrank, T. Nakajima, N. Mooren, A. Scheurer, H. Maid, F. Hampel, C. Trieflinger, J. Daub, *Eur. J. Inorg. Chem.* **2005**, 1149 – 1153; g) G. L. Abbati, A. Cornia, A. C. Fabretti, A. Caneschi, D. Gatteschi, *Inorg. Chem.* **1998**, *37*, 3759 – 3766; h) S. Koizumi, M. Nihei,

T. Shiga, M. Nakano, H. Nojiri, R. Bircher, O. Waldmann, S. T. Ochsenbein, H. U. Güdel, F. Fernandez-Alonso, H. Oshio, *Chem. Eur. J.* **2007**, *13*, 8445 – 8453; i) S. Koizumi, M. Nihei, M. Nakano, H. Oshio, *Inorg. Chem.* **2005**, *44*, 1208 – 1210; j) R. W. Saalfrank, A. Scheurer, R. Prakash, F. W. Heinemann, T. Nakajima, F. Hampel, R. Leppin, B. Pilawa, H. Rupp, P. Muller, *Inorg. Chem.* **2007**, *46*, 1586 – 1592; k) T. Liu, B.-W. Wang, Y.-H. Chen, Z.-M. Wang, S. Gao, *Z. Anorg. Allg. Chem.* **2008**, *634*, 778 – 783.

[11] S.-H. Zhang, C. Feng, *J. Mol. Struct.* **2010**, *977*, 62 – 66.

[12] a) X.-T. Wang, B.-W. Wang, Z.-M. Wang, W. Zhang, S. Gao, *Inorg. Chim. Acta* **2008**, *361*, 3895 – 3902; b) A. Ferguson, A. Parkin, J. Sanchez-Benitez, K. Kamenev, W. Wernsdorfer, M. Murrie, *Chem. Commun.* **2007**, 3473 – 3475.

[13] a) S. Mukherjee, R. Bagai, K. A. Abboud, G. Christou, *Inorg. Chem.* **2011**, *50*, 3849 – 3851; b) H. Oshio, N. Hoshino, T. Ito, M. Nakano, F. Renz, P. Gütlich, *Angew. Chem.* **2003**, *115*, 233 – 235; *Angew. Chem. Int. Ed.* **2003**, *42*, 223 – 225; c) L. F. Jones, P. Jensen, B. Moubaraki, K. J. Berry, J. F. Boas, J. R. Pilbrow, K. S. Murray, *J. Mater. Chem.* **2006**, *16*, 2690 – 2697.

[14] a) S. T. Meally, G. Karotsis, E. K. Brechin, G. S. Papaefstathiou, P. W. Dunne, P. McArdle, L. F. Jones, *CrystEngComm* **2010**, *12*, 59 – 63; b) S.-H. Zhang, N. Li, C.-M. Ge, C. Feng, L.-F. Ma, *Dalton Trans.* **2011**, *40*, 3000 – 3007.

[15] M. Manoli, A. Collins, S. Parsons, A. Candini, M. Evangelisti, E. K. Brechin, *J. Am. Chem. Soc.* **2008**, *130*, 11129 – 11139.

[16] A. K. Powell, S. L. Heath, D. Gatteschi, L. Pardi, R. Sessoli, G. Spina, F. Del Giallo, F. Pieralli, *J. Am. Chem. Soc.* **1995**, *117*, 2491 – 2502.

[17] E. K. Brechin, S. G. Harris, A. Harrison, S. Parsons, A. Gavin Whittaker, R. E. P. Winpenny, *Chem. Commun.* **1997**, 653 – 654.

[18] C. J. Milios, M. Manoli, G. Rajaraman, A. Mishra, L. E. Budd, F. White, S. Parsons, W. Wernsdorfer, G. Christou, E. K. Brechin, *Inorg. Chem.* **2006**, *45*, 6782 – 6793.

[19] S. K. Langley, N. F. Chilton, B. Moubaraki, K. S. Murray, *Dalton Trans.* **2012**, *41*, 9789 – 9796.

[20] S. K. Langley, N. F. Chilton, M. Massi, B. Moubaraki, K. J. Berry, K. S. Murray, *Dalton Trans.* **2010**, *39*, 7236 – 7249.

[21] A. Bencini, F. Totti, *Int. J. Quantum Chem.* **2005**, *101*, 819 – 825.

[22] L. Noodleman, *J. Chem. Phys.* **1981**, *74*, 5737 – 5743.

[23] a) P. Christian, G. Rajaraman, A. Harrison, J. J. W. McDouall, J. T. Raftery, R. E. P. Winpenny, *Dalton Trans.* **2004**, 1511 – 1512; b) G. Rajaraman, E. Ruiz, J. Cano, S. Alvarez, *Chem. Phys. Lett.* **2005**, *415*, 6 – 9; c) M. L. Baker, G. A. Timco, S. Piligkos, J. S. Mathieson, H. Mutka, F. Tuna, P. Kozlowski, M. Antkowiak, T. Guidi, T. Gupta, H. Rath, R. J. Woolfson, G. Kamieniarz, R. G. Pritchard, H. Weihe, L. Cronin, G. Rajaraman, D. Collison, E. J. L. McInnes, R. E. P. Winpenny, *Proc. Natl. Acad. Sci. USA* **2012**, *109*, 19113 – 19118; d) G. Rajaraman, J. Cano, E. K. Brechin, E. J. L. McInnes, *Chem. Commun.* **2004**, 1476 – 1477.

[24] a) E. Ruiz, J. Cano, S. Alvarez, A. Caneschi, D. Gatteschi, *J. Am. Chem. Soc.* **2003**, *125*, 6791 – 6794; b) G. Rajaraman, K. E. Christensen, F. K. Larsen, G. A. Timco, R. E. P. Winpenny, *Chem. Commun.* **2005**, 3053 – 3055.

[25] S. Ghosh, S. K. Singh, S. Tewary, G. Rajaraman, *Dalton Trans.* **2013**, *42*, 16490 – 16493.

[26] A. D. Becke, *J. Chem. Phys.* **1993**, *98*, 5648 – 5652.

[27] A. Schäfer, C. Huber, R. Ahlrichs, *J. Chem. Phys.* **1994**, *100*, 5829 – 5835.

[28] Gaussian 09, Revision A.02, M. J. Frisch, G. W. Trucks, H. B. Schlegel, G. E. Scuseria, M. A. Robb, J. R. Cheeseman, G. Scalmani, V. Barone, B. Mennucci, G. A. Petersson, H. Nakatsuji, M. Caricato, X. Li, H. P. Hratchian, A. F. Izmaylov, J. Bloino, G. Zheng, J. L. Sonnenberg, M. Hada, M. Ehara, K. Toyota, R. Fukuda, J. Hasegawa, M. Ishida, T. Nakajima, Y. Honda, O. Kitao, H. Nakai, T. Vreven, J. A. Montgomery, Jr., J. E. Peralta, F. Ogliaro, M. Bearpark, J. J. Heyd, E. Brothers, K. N. Kudin, V. N. Staroverov, R. Kobayashi, J. Normand, K. Raghavachari, A. Rendell, J. C. Burant, S. S. Iyengar, J. Tomasi, M. Cossi, N. Rega, J. M. Millam, M. Klene, J. E. Knox, J. B. Cross, V. Bakken, C. Adamo, J. Jaramillo, R. Gomperts, R. E. Stratmann, O. Yazyev, A. J. Austin, R. Cammi, C. Pomelli, J. W. Ochterski, R. L. Martin, K. Morokuma, V. G. Zakrzewski, G. A. Voth, P. Salvador, J. J. Dannenberg, S. Dapprich, A. D. Daniels, O. Farkas, J. B. Foresman, J. V. Ortiz, J. Cioslowski, D. J. Fox, Gaussian Inc., Wallingford CT, **2009**.

[29] N. F. Chilton, R. P. Anderson, L. D. Turner, A. Soncini, K. S. Murray, *J. Comput. Chem.* **2013**, *34*, 1164 – 1175.

[30] F. Neese, *WIREs Comput. Mol. Sci.* **2012**, *2*, 73 – 78.

[31] a) S. K. Singh, G. Rajaraman, *Chem. Eur. J.* **2014**, *20*, 5214 – 5218; b) N. Berg, T. N. Hooper, J. Liu, C. C. Beedle, S. K. Singh, G. Rajaraman, S. Piligkos, S. Hill, E. K. Brechin, L. F. Jones, *Dalton Trans.* **2013**, *42*, 207 – 216; c) S. K. Singh, G. Rajaraman, *Chem. Eur. J.* **2014**, *20*, 113 – 123; d) S. K. Singh, T. Gupta, P. Badkur, G. Rajaraman, *Chem. Eur. J.* **2014**, *20*, 10305 – 10313.

[32] a) S. Sanz, J. M. Frost, T. Rajeshkumar, S. J. Dalgarno, G. Rajaraman, W. Wernsdorfer, J. Schnack, P. J. Lusby, E. K. Brechin, *Chem. Eur. J.* **2014**, *20*, 3010 – 3013; b) A. Das, F. J. Klinke, S. Demeshko, S. Meyer, S. Dechert, F. Meyer, *Inorg. Chem.* **2012**, *51*, 8141 – 8149.

[33] N. A. Law, J. W. Kampf, V. L. Pecoraro, *Inorg. Chim. Acta* **2000**, *297*, 252 – 264.

[34] a) A. Prescimone, J. Sanchez-Benitez, K. V. Kamenev, S. A. Moggach, A. R. Lennie, J. E. Warren, M. Murrie, S. Parsons, E. K. Brechin, *Dalton Trans.* **2009**, 7390 – 7395; b) A. Prescimone, J. Wolowska, G. Rajaraman, S. Parsons, W. Wernsdorfer, M. Murugesu, G. Christou, S. Piligkos, E. J. L. McInnes, E. K. Brechin, *Dalton Trans.* **2007**, 5282 – 5289.

[35] a) A. Bencini, D. Gatteschi, M. Mattesini, F. Totti, I. Ciofini, *Mol. Cryst. Liq. Cryst. Sci. Technol. Sect. A* **1999**, *335*, 665 – 674; b) M. Orio, D. A. Pantazis, T. Petrenko, F. Neese, *Inorg. Chem.* **2009**, *48*, 7251 – 7260; c) C. D. Delfs, R. Stranger, *Inorg. Chem.* **2001**, *40*, 3061 – 3076; d) Y. H. Lu, H. K. Fun, S. Chantrapromma, I. A. Razak, Z. Shen, J. L. Zuo, X. Z. You, *Acta Crystallogr. Sect. C* **2001**, *57*, 911 – 913.

Received: October 16, 2014
Published online on December 18, 2014

